Coupling between phonons and magnetic excitations in orthorhombic $Eu_{1-x}Y_xMnO_3$

J. Agostinho Moreira,* A. Almeida, W. S. Ferreira, J. E. Araújo, A. M. Pereira, and M. R. Chaves
Departamento de Física, IFIMUP and IN-Institute of Nanoscience and Nanotechnology, Faculdade de Ciências, Universidade do Porto, Rua do Campo Alegre 687, 4169-007 Porto, Portugal

J. Kreisel
Laboratoire des Matériaux et du Génie Physique, Grenoble Institute of Technology, CNRS, 38016 Grenoble, France

S. M. F. Vilela and P. B. Tavares
Centro de Química, Universidade de Trás-os-Montes e Alto Douro, Apartado 1013, 5001-801 Vila Real, Portugal
(Received 27 March 2009; revised manuscript received 10 January 2010; published 26 February 2010)

In this work we present a detailed study of the structural and lattice-dynamic properties of Y-doped $EuMnO_3$ ceramics ($Eu_{1-x}Y_xMnO_3$ with $0 \leq x \leq 0.5$). A thorough analysis toward the correlation between both structural and Raman modes parameters has been undertaken. Our results provide evidence for two main structural distortions of MnO_6 octahedra, arising from a cooperative Jahn-Teller and rotational distortions in these compounds. The temperature dependence of the B_{1g} symmetric stretching mode of the MnO_6 units has revealed either a positive or negative shift regarding the pure anharmonic temperature dependence of the phonon frequency, which strongly depends on the Y concentration. This frequency renormalization is explained in terms of a competition between ferromagnetic and antiferromagnetic interactions. Frequency shifts observed well above the Néel temperature are likely associated with the coupling between phonons and electromagnons, which provides further grounds for the existence of strong spin-phonon coupling in this compound. Both polar and magnetoelectric properties ascertained for $x=0.2$ provide clear evidence of the central role played by spin-phonon coupling in yielding the physical behavior of the Y-doped $EuMnO_3$ system.

DOI: 10.1103/PhysRevB.81.054447 PACS number(s): 75.80.+q, 63.20.−e, 75.30.Et, 77.22.−d

I. INTRODUCTION

Magnetoelectric multiferroic materials, exhibiting coupled ferroelectric and ferromagnetic orders parameters, are attractive for future technological applications, such as a new generation of both electrically and magnetically controlled multifunctional devices. Unfortunately, the number of such materials remains scarce.[1] On the other hand, materials presenting coupled ferroelectric and antiferromagnetic (AFM) properties are more frequent, and they are just known as magnetoelectric materials.[2] Among them, rare-earth manganites have drawn an important interest in the scientific community due to their rich phase diagram and the associated microscopic mechanisms of which the understanding remains challenging.

In conventional ferroelectrics, such as $BaTiO_3$, hybridization between the titanium $3d$ states and the oxygen $2p$ states is essential for proper ferroelectricity.[3] Ferroelectricity in magnetoelectric rare-earth manganites is entirely different in nature, as it has an improper character, which has been attributed to the spin-lattice interactions in a modulated off-center symmetric magnetic structure.[4–6] In magnetoelectric rare-earth manganites an electric polarization has been only observed when they are cooled under high electric fields ($E > 1$ kV/cm),[7] and the saturation value of the polarization is rather small. It has been proposed that ferroelectricity can be originated from a variety of spiral magnetic structures,[4] and can be explained in terms of the inverse Dzyaloshinski-Morya model, where the electric polarization is expected as,[8,9]

$$\vec{P} = \sum_{i,j} A\vec{e}_{ij} \times (\vec{S}_i \times \vec{S}_j). \quad (1)$$

$\vec{e}_{ij}$ denotes the unit vector connecting the interacting neighbor $\vec{S}_i$ and $\vec{S}_j$ spins, and A is the coupling constant between electric polarization and magnetic momenta. As the electric polarization arises from lattice distortions, the study of the spin-phonon coupling is particularly notorious in the systems that present simultaneously magnetic and ferroelectric properties. However, spin-phonon, and thus magnetoelectric coupling has shown to be rather weak in to date studied materials, inhibiting their use in technical applications. Consequently, from both fundamental and application point of view, a further understanding of spin-phonon coupling remains an important issue.

A Raman-scattering study of orthorhombic rare-earth manganites ($ReMnO_3$) revealed a significant coupling between spins and lattice for compounds with Re=Pr, Nd, and Sm near and below the Néel temperature.[10] We note that the effect of the magnetic ordering is very weak or negligible in rare-earth manganites with Re=Gd, Tb, Dy, Ho, and Y, which are considered as magnetoelectric compounds.[10] Any comparative analysis of these compounds is rather complex because both the variations in the rare-earth radii and the different values of magnetic moment in different Re ions have to be taken into account.[11] This complexity is reduced in the $Eu_{1-x}Y_xMnO_3$ system ($0 \leq x \leq 0.5$), with an orthorhombic distorted perovskite structure of *Pbnm* symmetry, because the magnetic properties are entirely due to the manganese $3d$ spins, since Eu^{3+} and Y^{3+} present no magnetic momenta.[12] Further interest in this system comes from its

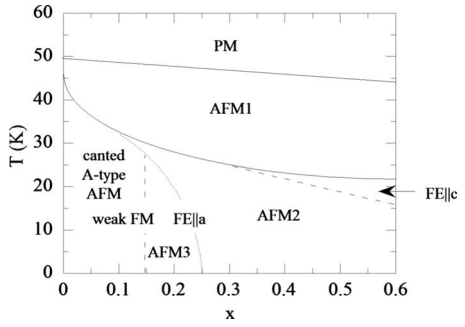

FIG. 1. (x,T) phase diagram of $Eu_{1-x}Y_xMnO_3$ $(0 \leq x \leq 0.55)$ obtained from the results described in Ref. 13.

(x,T) phase diagram, which shows a rich phase sequence at low temperatures, exhibiting different types of both polar and magnetic structures.[13] Due to the fact that the Y^{3+} radius (1.02 Å) is smaller than that of Eu^{3+} (1.09 Å), the orthorhombic distortion of the $Eu_{1-x}Y_xMnO_3$ increases with x, and can be quantified by the spontaneous orthorhombic strain factor,[14]

$$e = \frac{2(b-a)}{b+a}, \tag{2}$$

where a and b denote the values of the lattice parameters. This distortion is a consequence of the Jahn-Teller cooperative effect and the tilting of the octahedra around the a axis, thus lowering the symmetry of the system.[14] As a consequence of this increasing lattice deformation, the orbital overlap becomes larger via the Mn-O(I)-Mn bond angle and, in turn the electronic properties of the system are modified.[15]

In this paper we present a detailed study of the crystal structure and lattice dynamics at room temperature, and of the spin-phonon coupling in $Eu_{1-x}Y_xMnO_3$ in the concentration range $0 \leq x \leq 0.5$, by using both x-ray powder diffraction and Raman spectroscopy. In particular, we aim at correlating the Raman-active modes with the lattice distortions in this system, and to determine the relevance of the interaction between magnetic spins and internal vibrations to the onset of electric polarization. Moreover, both polar and magnetoelectric properties for the composition with $x=0.2$ are presented in order to figure out the role of spin-phonon coupling in $Eu_{1-x}Y_xMnO_3$.

II. PHASE DIAGRAM OF $Eu_{1-x}Y_xMnO_3$

Let us first discuss the literature work which is relevant for the interpretation and understanding of our own experimental results. Based on magnetic and dielectric measurements, as well as on heat-capacity studies a detailed (x,T) phase diagram has been proposed for $Eu_{1-x}Y_xMnO_3$, which is shown in Fig. 1.[13] The paramagnetic phase above the Néel temperature, $T_N \approx 50-45$ K, is followed by an antiferromagnetic phase (AFM1). By analogy with others $ReMnO_3$ compounds $(Re=Ho,Dy,Tb,Gd,Eu)$, Hemberger *et al.*[13] proposed a sinusoidal modulation for the AFM1 phase, which was confirmed experimentally by Yamasaki *et al.*,[16] for $x=0.2$, 0.3, and 0.4, using synchrotron radiation. For $x<0.15$, a new antiferromagnetic phase, with weakly ferromagnetic character, is established below $T_1 \approx 42-30$ K.[13,16] Taking into account the absence of ferroelectric polarization in this magnetic phase, it has been proposed that an A-type collinear spin structure is established.[13,16] For $0.15 \leq x < 0.3$, the system exhibits simultaneously a canted antiferromagnetism and an electric polarization along the a axis below $T_1 \approx 30$ K.[13] Yamasaki *et al.*[16] showed experimentally, that for the special case of $x=0.2$, the superlattice reflections observed in the AFM1 phase disappear below 30 K. Based on this result, these authors have proposed a ferromagnetic alignment of the Mn spins in the ab plane, without modulation, coupled antiferromagnetically along the c axis, where the magnetization appears.[16] Contradictory results have been obtained for the polar character of the low-temperature magnetic phase for $x=0.2$. While Hemberger *et al.*[13] found a finite electric polarization, Yamasaki *et al.*[16] reported the absence of any polar order in samples when measured with silver paste electrodes and under an electric field of 2 kV/cm. Yamasaki *et al.*[16] assigned the discrepancy between their result and the one reported by Hemberger *et al.*,[13] to the nonstoichiometry of the samples studied by these authors. For $x>0.25$, a modulated antiferromagnetic phase (AFM2) is observed below $T_1 \approx 28-22$ K, along with a ferroelectric polarization. The modulation wave vector depends on the Y content. According to the results obtained by Yamasaki *et al.*,[16] for $x=0.3$, a commensurate antiferromagnetic phase $(q_1=0.5)$ is observed, while for $x=0.4$ an incommensurate antiferromagnetic phase, with $q_1 \approx 0.56$ is established. For $0.4 \leq x \leq 0.5$, an electric polarization along the a or the c axis, depending on the temperature of the sample, is observed. The ferroelectricity in $Eu_{1-x}Y_xMnO_3$ $(x \geq 0.2)$ may have an improper character and could be attributed to a spin-lattice interaction in the modulated off-center symmetric magnetic structure.

The analysis of the experimental study of infrared transmittance in the terahertz and far infrared regions $(3 \leq \omega \leq 250\ cm^{-1})$ of $Eu_{1-x}Y_xMnO_3$ (with $x=0.2$, 0.3, and 0.5) evidenced clear anomalies in the dielectric constant around 35 K.[17,18] The magnitude of this effect is associated with the strength of the coupling between optically active phonons and spin waves. These excitations interact strongly with electromagnetic waves of adequate wavelengths and are called electromagnons. Electromagnetic waves can provide in $Eu_{1-x}Y_xMnO_3$ a contribution to the static dielectric constant in magnetic ordered phases. For $x=0.25$ the electromagnons observed are suppressed by external magnetic fields, which induce a canted antiferromagnetic phase.[17] In addition to electromagnons a broad contribution in the infrared transmission spectra is observed for $x=0.25$ in the definite polarization $e \| a$ and $h \| b$, and persists to temperatures as high as 150 K.[17] Above T_1, the low-frequency response has origin in this background. At $T=10$ K, the background accounts for approximately 50% for the total low-frequency oscillator strength below 140 cm^{-1}.[17] The gradual decrease in this background with temperature above T_N suggests that magnetic fluctuations are the origin of this behavior. It has been proposed that this background arises from the coupling of the phonons to dynamic fluctuations of the magnetic system in the paramagnetic phase.[17]

III. EXPERIMENTAL DETAILS

Details of the sample processing are available in Ref. 19. The phase purity, the crystallographic and the microstuctural characterization of the ceramic samples were checked using x-ray powder diffraction and scanning electron microscopy with energy-dispersive spectroscopy. The Rietveld analysis of the x-ray diffraction data shows the absence of secondary phases with occupancy factors converging to the nominal composition of the samples. This result was also confirmed by energy-dispersion spectroscopy. Scanning electron microscopy analysis reveals in both systems a typical ceramic microstructure with regular shaped crystal grains ranging from 3 up to 10 μm in diameter. The Rietveld analysis of the room-temperature x-ray data has enabled us to calculate the cell parameters, cell volume, bond lengths, and bond angles as a function of the Y concentration.

The Raman-scattering studies were performed with polished pellets ($3\times4\times5$ cm^3). The samples were placed in a closed-cycle helium cryostat (10–300 K temperature range) with a temperature stability of about ±0.2 K. The temperature homogeneity in the samples was achieved with a cooper mask setup. The temperature of the sample was estimated to differ by less than 1 K from the temperature measured with a silicon diode attached to the sample holder.

The unpolarized Raman spectra of $Eu_{1-x}Y_xMnO_3$ have been measured in the pseudobackscattering geometry, on cooling runs. The 632.8 nm polarized line of a He-Ne laser was used for excitation with an incident power of about 5 mW impinging on the sample. The scattered light was analyzed using a T64000 Jobin-Yvon spectrometer, operating in triple subtractive mode, and equipped with liquid nitrogen cooled charge-coupled device and photon-counting device. Identical conditions were maintained for all scattering measurements. The spectral slit width was about 1.5 cm^{-1}.

The sum of independent damped harmonic oscillators, according to the general formula,[20]

$$I(\omega,T)=[1+n(\omega,T)]\sum_{j=1}^{N}A_{oj}\frac{\omega\Omega_{oj}^2\Gamma_{oj}}{(\Omega_{oj}^2-\omega^2)^2+\omega^2\Gamma_{oj}^2} \quad (3)$$

was fitted to the experimental data. Here $n(\omega,T)$ is the Bose-Einstein factor; A_{oj}, Ω_{oj}, and Γ_{oj} are the strength, wave number, and damping coefficient of the jth oscillator, respectively.

Polar properties were ascertained by using inversion polarization and pyroelectric current techniques. Moreover, magnetoelectric properties were studied with a Quantum Design superconducting quantum interference device magnetometer, wherein the induced magnetization was measured after poling the sample with a dc electric field. The resolution in the magnetization measurements is better than 5×10^{-7} emu. Details of the experimental conditions are available in Refs. 21 and 22.

IV. EXPERIMENTAL RESULTS

A. Structure and lattice dynamics at room temperature

1. X-ray diffraction studies

Figure 2 shows an ORTEP plot of the unit cell of $EuMnO_3$ at room temperature. The $Eu_{1-x}Y_xMnO_3$ crystals, with $x\leq0.5$, present the same *Pbnm* orthorhombic structure, with $Z=4$, at 300 K, and are formed by a network of corner-sharing MnO_6 octahedra developing chains along the c axis, belonging to the family of rotationally distorted perovskites. The Eu^{3+} or Y^{3+} ions occupy the interstices between octahedra. Two main distortions have been evidenced from the analysis of the x-ray spectra, which will be presented in the following.

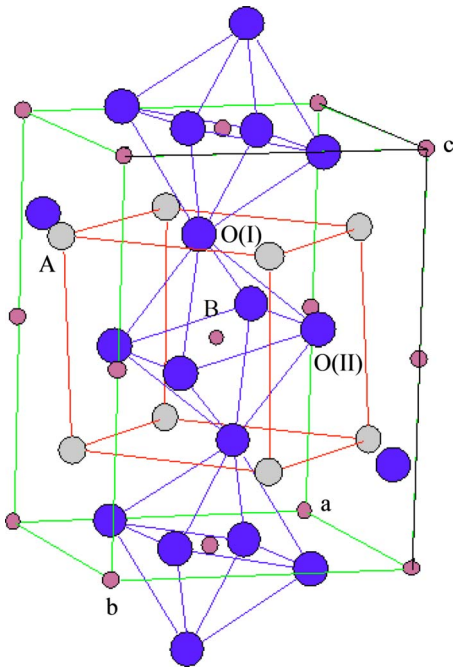

FIG. 2. (Color online) ORTEP plot of the $EuMnO_3$. The A denotes the rare-earth or Y^{3+} ions, the B denotes the Mn^{3+} ions, O(I) and O(II) denote the apical and equatorial O^{2-} ions, respectively.

The cell parameters and the cell volume as a function of x, obtained from the analysis of the x-ray diffraction data, are shown in Fig. 3(a). For all samples here studied, the lattice parameters fulfill the $c/\sqrt{2}<a<b$ relation, which is characteristic of the so-called O′ structure, typically found in other rare-earth manganites presenting distortions of the octahedral environment of the Mn^{3+} ions, associated with a strong Jahn-Teller distortion of the MnO_6 units and orbital ordering.[14,23] The increase in Y concentration with a smaller ionic radius than Eu^{3+} leads to a decrease in both cell parameters and volume, actually due to the decrease in the effective A-site volume. As it can be seen from Fig. 3(a), the slope of the straight line $b(x)$ parameter ($\Delta b/\Delta x=-0.04\pm0.01$ Å) is smaller than the ones of $a(x)$ and $c(x)$ ($\Delta a/\Delta x=-0.084\pm0.001$ Å, $\Delta c/\Delta x=-0.067\pm0.003$ Å), as it has been observed in other rare-earth manganites. This kind of behavior has been attributed to the tilting of MnO_6 octahedra in *Pbnm* perovskite structure, of the type $\bar{a}\bar{a}c^+$ in Glazer´s notation,[24] for which the distortion driven by a reduction in the A-site volume leaves b slightly x dependent. The spontaneous orthorhombic strain (e) as a function of x is depicted in Fig. 3(b). The e parameter, which characterizes the orthorhombic distortion of the lattice [Eq. (2)], increases monotonically with x, corroborating the increasing deformation of the lattice with respect to the ideal cubic perovskite structure.

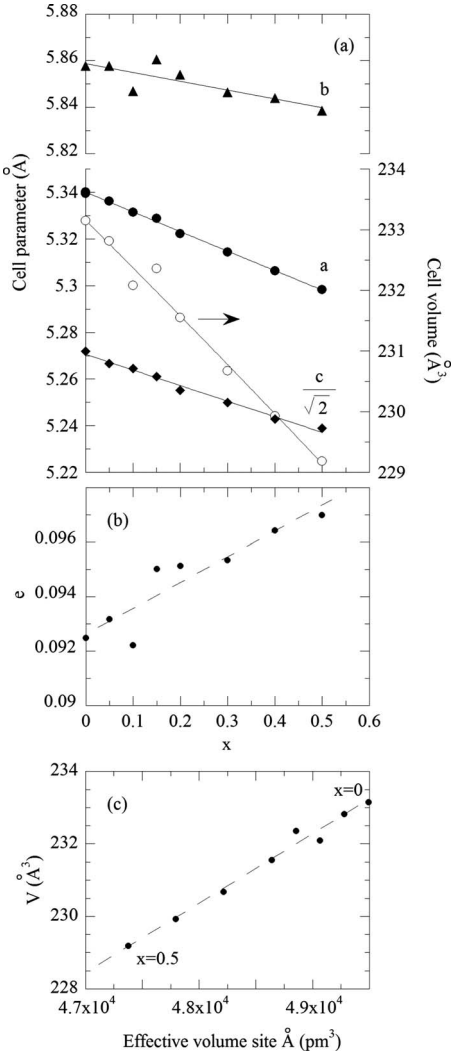

FIG. 3. (a) Lattice parameters and cell volume of $Eu_{1-x}Y_xMnO_3$, as a function of x. (b) Spontaneous orthorhombic strain as a function of x. (c) Cell volume versus the effective volume of the A site.

The increase in the spontaneous orthorhombic strain e provides a clear evidence for a continuous octahedra tilting and also measures the distortion of the octahedra: both effects are simultaneously observed in several $ReMnO_3$, which lead to changes in the lattice parameters, and significant distortions of the Mn-O(I)-Mn angles.[25] The observed decrease in the cell volume scales very well with the effective A-site volume, as it can be seen in Fig. 3(c). It is interesting to remind that the decreasing in the cell volume strongly influences the magnetic exchange and the electronic orbital overlapping and, in this way, the magnetic properties of these materials, as it has been observed in other rare-earth manganites.[15]

From Rietveld refinement of the atomic positions, we have calculated the values of both the length and angle of chemical bonds involved in the MnO_6 octahedra, the R-O(I) distances and the octahedra tilt angle for each value of x. Figure 4 shows the R-O(I) and Mn-O bond lengths, and the octahedra tilt angle as a function of the Y concentration. Two different R-O(I) lengths have been detected for all the considered compositions. While for low Y concentrations ($x \leq 10$) the R-O(I) lengths are practically constant, a slightly decrease is observed as x increases for higher Y concentrations. In the range $0.15 \leq x \leq 0.4$, the difference between the two R-O(I) length values is more pronounced. The difference between both R-O(I) bond length values is likely associated with the behavior of the octahedra tilt angle.

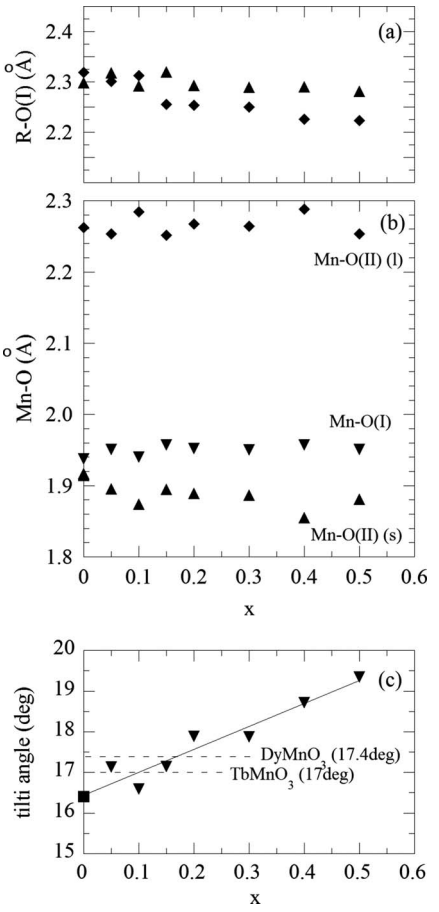

FIG. 4. Dependence of the (a) R-O(I), (b) Mn-O lengths, and tilt angle (c) on the Y content. In Fig. 4(b) the l and s denotes larger and smaller.

Significant distortions in the MnO_6 unit are detected from the analysis of the values of the Mn-O bond lengths. In fact, from the Rietveld refinement, we have found three different values for the Mn-O bond length for each composition, evidencing the existence of deformations of the MnO_6 unit. While only one value is found for the Mn-O(I) bond lengths, two different values for the Mn-O(II) ones are displayed, whose difference is about 20%. This result is also observed in other rare-earth manganites and is a consequence of the Jahn-Teller distortions which manifest themselves by a rather pronounced difference between the values of the Mn-O(II) bond lengths, roughly lying in the ab plane. In order to quantify the distortion of the octahedra, we have used the Δ_d parameter, defined as,[14]

$$\Delta_d = \frac{1}{6}\sum_{i=1}^{6}\left[\frac{d_i - \langle d\rangle}{\langle d\rangle}\right]^2, \quad (4)$$

TABLE I. Δ_d parameter [see Eq. (4)] for some rare-earth manganites. The values for $LaMnO_3$ and $PrMnO_3$ were obtained from Refs. 25 and 26.

Rare-earth ion	$\Delta_d \times 10^4$
La	33.1
Pr	43.1
Nd	49.9
Sm	50.2
Eu	51.9
Gd	48.7
Dy	44.9

where d=Mn-O and $\langle d \rangle$ is the mean value of Mn-O. We have also studied the crystal structure of other orthorhombic rare-earth manganites $ReMnO_3$, with Re=Nd, Sm, Eu, Gd, and Dy, and we have calculated for each one the corresponding value of the Δ_d parameter. Using the data obtained in this work, we have also determined the mean value of Δ_d for the $Eu_{1-x}Y_xMnO_3$ system. Table I shows the value of Δ_d obtained along with the ones calculated from the data presented in Refs. 25 and 26. As it can be seen, for undoped compounds, the Δ_d parameter increases monotonously as the ionic radius decreases, from $LaMnO_3$ ($\Delta_d = 33.1 \times 10^{-4}$), reaching the maximum value of 51.9×10^{-4} for $EuMnO_3$. On further decrease in the ionic radius, Δ_d decreases. However, for Y-doped $EuMnO_3$ system, the mean value of Δ_d is 67.3×10^{-4}, which is significantly larger than the values obtained for the other orthorhombic $ReMnO_3$ compounds. This result is a consequence of a substitution disorder induced by Y doping. In fact, due to the random distribution of the Y^{3+} ions in the lattice, different octahedra feel different environment; so, largest distortion are expected to be observed.

The tilt, defined as $[180°\text{-(Mn-O(I)-Mn)}]/2$,[26] reveals itself to be an important parameter as its value reflects the magnetic interactions responsible for the spin structure exhibited by the rare-earth manganites. As we can see from Fig. 4(c), the tilt angle increases monotonously with increasing x. The increase in the tilt angle with decreasing cell volume corroborates the continuous deviation from the cubic structure due to Y doping obtained in the previous results. It is interesting to stress that the values of the tilt angle observed in both $TbMnO_3$ and $DyMnO_3$, which exhibit strong magnetoelectric effects, are comparable with those obtained for $x \sim 0.15$ and 0.2, respectively.[14]

2. Raman spectroscopic studies

Unpolarized Raman spectra of $Eu_{1-x}Y_xMnO_3$, x=0, 0.1, 0.3, 0.4, and 0.5, recorded at room temperature are shown in Fig. 5.

In the orthorhombic rare-earth manganites, the activation of the Raman modes is due to deviations from the ideal cubic perovskite structure. Factor group analysis of the $EuMnO_3$ structure provides the following decomposition corresponding to the 60 normal vibrations at the Γ point of the Brillouin zone,

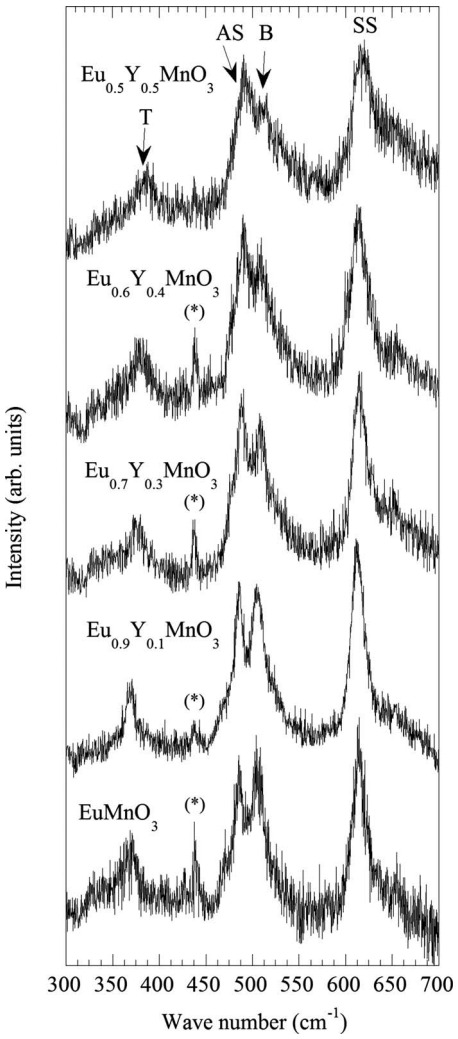

FIG. 5. Raman spectra of $Eu_{1-x}Y_xMnO_3$, for x=0, 0.1, 0.3, 0.4, and 0.5, recorded at room temperature. The laser plasma line is indicated by (*). Mode assignment: SS, symmetric stretching mode (symmetry B_{2g}); AS, Jahn-Teller-type asymmetric stretching mode (symmetry A_g); B, bending mode (symmetry B_{2g}); T, tilt mode of the MnO_6 octahedra (symmetry A_g).

$$\Gamma_{\text{acustic}} = B_{1u} + B_{2u} + B_{3u},$$

$$\Gamma_{\text{optical}} = (7A_g + 7B_{1g} + 5B_{2g} + 5B_{3g})_{\text{Raman active}} + (8A_u + 10B_{1u} + 8B_{2u} + 10B_{3u})_{\text{IR active}}.$$

The Raman-active modes preserve the inversion center, thus Mn^{3+} ions do not contribute to the Raman spectra. Due to the polycrystalline nature of the studied samples, our Raman spectra exhibit simultaneously all Raman-active modes A_g, B_{1g}, B_{2g}, and B_{3g}. Earlier reports by Lavèrdiere *et al.*,[10] propose that the more intense Raman bands are of A_g and B_{2g} symmetry, which has been used to allow the mode assignment presented in this work. In good agreement with this, our observed A_g and B_{2g} modes are the more intense bands in $Eu_{1-x}Y_xMnO_3$. As these modes are the relevant ones for our study, we are convinced that using ceramics instead of single crystals, no relevant information is loosed regarding

the correlation between normal modes and structural deformations, the temperature dependence of the mode parameters, and so, the coupling between spins and phonons. Contrarily to other ceramic systems, such as $SrTiO_3$, the activation of infrared modes due to the symmetry breaking in the grain boundaries is not observed in our Raman spectra.[27] Figure 5 shows that the spectral signature of all $Eu_{1-x}Y_xMnO_3$ (with $x \leq 0.5$) compounds is qualitatively similar in the 300–800 cm^{-1} frequency range in terms of frequency, linewidth, and intensity. The similarity of the Raman signatures suggests that all studied powders present at ambient conditions the same space group and that the internal modes of the MnO_6 octahedra units are not substantially affected by the Y doping.

Nevertheless, a closer quantitative analysis of the spectra shows subtle changes as a function of the substitution rate. For instance, the broad feature located at around 520 cm^{-1} becomes more pronounced as the Y concentration increases. Also, the frequency of the band located close to 364 cm^{-1} does significantly increase with increasing x.

A detailed study, published by Martín-Carrón *et al.*,[28] concerning the dependence of the frequency of the Raman bands in some stoichiometric rare-earth manganites $ReMnO_3$, enables us to assign the more intense Raman bands in our spectra. In $Eu_{1-x}Y_xMnO_3$ the band at 613 cm^{-1} is associated with a symmetric stretching mode involving the O(II) atoms (symmetry B_{2g}),[28–31] the band at 506 cm^{-1} to a bending mode (symmetry B_{2g}), the band at 484 cm^{-1} to a Jahn-Teller type asymmetric stretching mode involving also the O(II) atoms (symmetry A_g), and the band at 364 cm^{-1} to a bending mode of the tilt of the MnO_6 octahedra (symmetry A_g).

On the basis of these assignments, it is now interesting to correlate the x dependence of the frequency of these Raman bands with the structural changes induced by the Y doping. The more noticeable stretching modes in $ReMnO_3$ are known to involve nearly pure Mn-O(II) bond and they are found to be slightly dependent on the chemical pressure. In orthorhombic rare-earth manganites, the stretching modes change less than 5 cm^{-1} with the rare-earth substitution, from La to Dy.[29] Figure 6 shows the evolution of the two bands located around 613 and 484 cm^{-1}. The observed frequency changes of only 2 cm^{-1} when x increases from 0 to 0.5, correlates well with a weak dependence of the Mn-O(II) bond lengths with x [see Fig. 4(b)]. The weak x dependence of the frequency of these modes provides further evidence for a slight dependence of the MnO_6 octahedron volume and Mn-O bonds lengths on the Y doping, in agreement with literature work on other rare-earth manganites.[28] The remaining two modes B and T depicted in Fig. 6, exhibit a large variation with x (about 10–15 cm^{-1} when x varies from 0 to 0.5), which correlates rather well with the x dependence of the tilt angle. The lower frequency T mode exhibits the largest variations with x, and it is actually associated with an external mode A_g with origin in the tilt mode of the MnO_6. A linear dependence of the frequency of T mode in the tilt angle is observed from Fig. 7. The slope of the linear relation is 5 cm^{-1}/deg, which is a very small value when compared with the one obtained for the same mode in other orthorhombic manganites (23 cm^{-1}/deg).[29] Mode B is assigned to the bending mode B_{2g} of the octahedra.[27] The two broad shoulders observed at round 470 and 520 cm^{-1} are likely the B_{2g} in-phase O(II) scissorlike and out-of-plane MnO_6 bending modes.

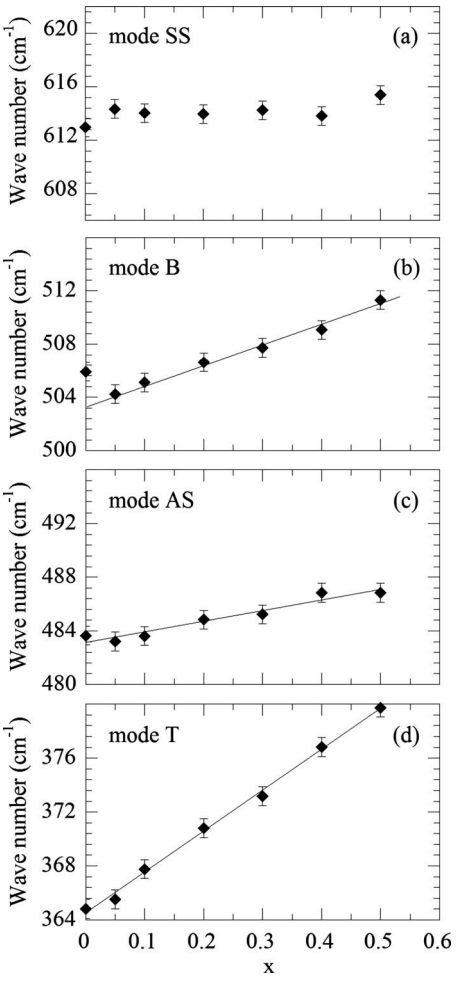

FIG. 6. Dependence of the frequency of the (a) symmetric stretching mode (SS), (b) bending mode (B), (c) antisymmetric stretching mode (AS), and (d) tilt mode (T), on the Y content. The solid lines are guides for the eyes.

The increase in Y concentration provides evidence for some modifications in the crystal structure, which manifest themselves through changes in the mode frequencies, relative intensities, and linewidths. The most interesting

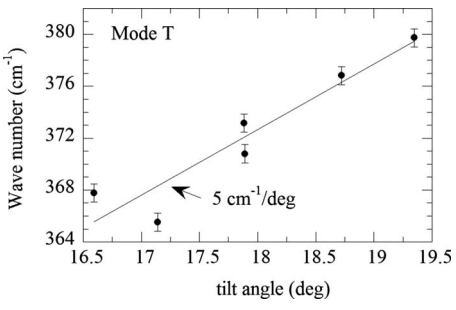

FIG. 7. Variation with the tilt angle of the frequency of the T mode. The solid line was obtained from the best fit of the linear function to the experimental data.

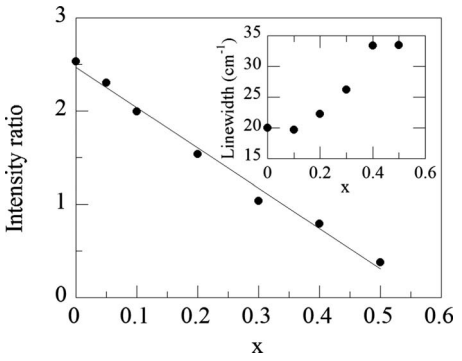

FIG. 8. The ratio between the intensities of the bending and asymmetric stretching modes, as a function of the Y content. Inset: linewidth of the symmetric stretching mode versus Y content.

example concerns the intensity interchange between the bending and asymmetric stretching modes (spectral range 470–520 cm^{-1}) and the damping coefficient of the symmetric stretching mode. The ratio between the intensity of the bending and the asymmetric stretching modes is presented in Fig. 8, where a linear decrease in the intensity ratio as the Y concentration increases is observed. This effect has been also observed in the same spectral range for the whole rare-earth manganite series, and it has been associated with the coupling between these two modes, which is stronger for *Re* =Eu, Gd, and Tb.[29] The inset of Fig. 8 shows the linewidth of the symmetric stretching modes as a function of the Y concentration. An increase in the linewidth with increasing x is observed due to the structural disorder arising from the partial substitution of Eu^{3+} by Y^{3+}.

B. Temperature dependence of the Raman spectra

Figure 9 shows the unpolarized Raman spectra of $EuMnO_3$, $Eu_{0.8}Y_{0.2}MnO_3$, and $Eu_{0.5}Y_{0.5}MnO_3$, recorded at 200 and 9 K. As it can be seen in Figs. 9(a)–9(c), the spectra at 200 and 9 K show only very small changes in their profiles. Particularly, no new bands were detected at low temperatures. The absence of well-defined activated Raman bands, even for the composition where a spontaneous ferroelectric order is expected, may have origin in two different mechanisms: the maintenance of the inverse center or the weak polar character of the ferroelectric phases for $x \geq 0.2$.

Nevertheless, the detailed analysis of the spectra reveals the presence of anomalies in the temperature dependence of some phonon parameters across the magnetic phase transitions. As an example, Fig. 10 shows the Raman spectra of $Eu_{0.8}Y_{0.2}MnO_3$, recorded at several fixed temperatures, in the 590–640 cm^{-1} spectral range. As we can see from Fig. 10, the frequency of the symmetric stretching mode exhibit intriguing temperature behavior, hardening as the temperature decreases from room temperature toward 100 K, then softening as the temperatures further decreases. Such behavior provides evidence for some kind of structural rearrangement or coupling.

According to the spin-phonon coupling models, one should expect detectable changes in the phonon frequencies on entering the magnetic phases, reflecting the phonon renormalization, proportional to the spin-spin correlation function for the nearest Mn^{3+} spins. Aiming at searching for a spin-phonon coupling in $Eu_{1-x}Y_xMnO_3$ series, we have monitored in detail the temperature dependence of the parameters characterizing the MnO_6 Raman-active modes. Among them, we have found that the symmetric stretching mode (SS) around 615 cm^{-1} is the most sensitive to the magnetic order. In fact, this mode affects the geometrical parameters associated with the spontaneous orthorhombic strain e and, so a strong coupling between the SS mode and the electronic degrees of freedom is expected. In other rare-earth manganites, such as Ca-doped $PrMnO_3$, this mode is so strongly coupled with the electronic system that it can be used to control a metal-insulator transition, by its coherent manipulation through selective-mode excitation.[32] The temperature dependence of the frequency of the symmetric stretching mode for the different studied chemical compositions is shown in Fig. 11, together with the insets, which present the temperature dependence of the corresponding linewidths.

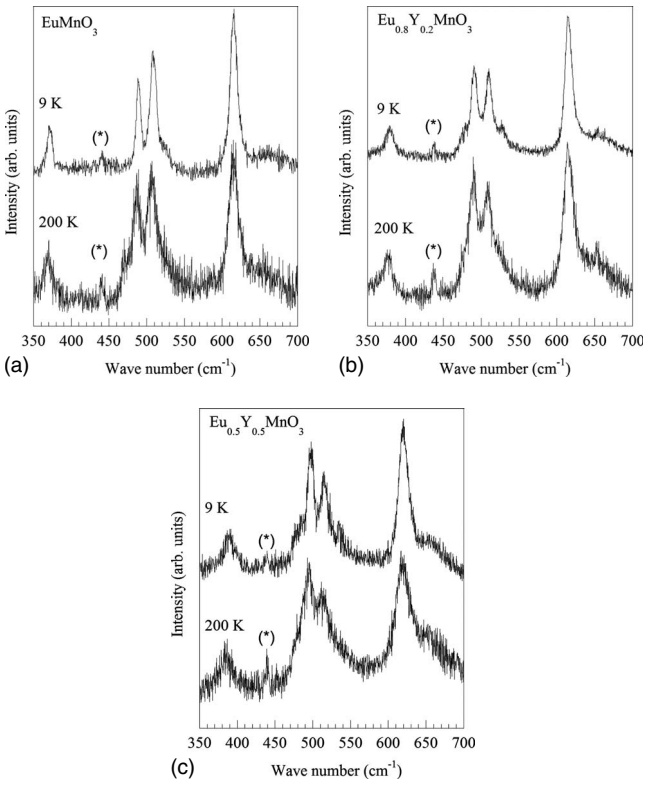

FIG. 9. The Raman spectra of (a) $EuMnO_3$, (b) $Eu_{0.8}Y_{0.2}MnO_3$, and (c) $Eu_{0.5}Y_{0.5}MnO_3$, recorded at 200 and at 9 K. The laser plasma line is indicated by (*).

In order to calculate the influence of the magnetic exchange interactions on the phononic behavior, we describe the purely anharmonic temperature dependence of the frequency and of the linewidth of the different modes by the model,[33]

$$\omega(T) = \omega(0) + C\left(1 - \frac{2}{e^x - 1}\right), \tag{5}$$

for the temperature dependence of the frequency of the transverse mode and,[33]

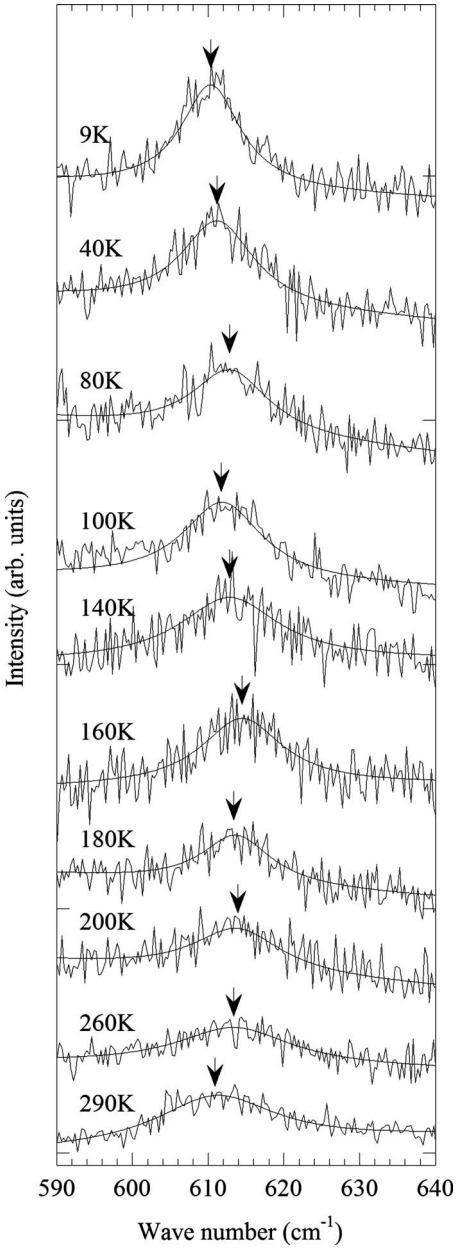

FIG. 10. Raman spectra of $Eu_{0.8}Y_{0.2}MnO_3$ recorded at several fixed temperatures in the 590–640 cm^{-1} spectral range. The solid lines were obtained from the best fit of Eq. (3) to the spectra.

$$\Gamma(T) = \Gamma(0)\left(1 + \frac{2}{e^x - 1}\right) \tag{6}$$

for the temperature dependence of its linewidth. In Eqs. (5) and (6), $\omega(T)$ and $\omega(0)$ is the frequency of the optical mode at the temperature T and 0 K, respectively, $x = \frac{\hbar\omega_o}{2k_BT}$, where ω_o is the characteristic frequency of the mode, $\Gamma(T)$ and $\Gamma(0)$ are the linewidths of the mode at the temperature T and 0 K, respectively.[33] The solid lines in Fig. 11 correspond to the best fit of these equations to the high-temperature range data ($T > 100$ K), with the adjustable parameters C, $\omega(0)$, $\Gamma(0)$, and ω_o.

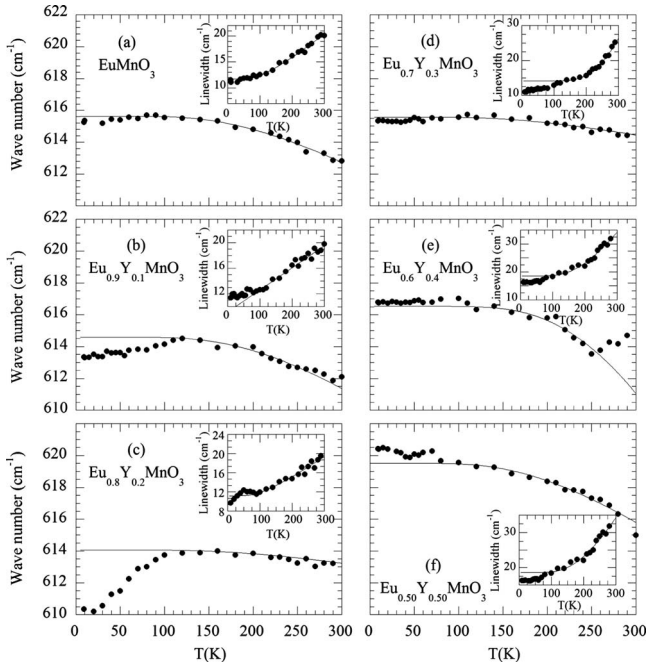

FIG. 11. Temperature dependence of the Raman frequency of the symmetric stretching mode of MnO_6 octahedra. The insets show the temperature dependence of the linewidths; the solid lines have been obtained from the best fit of Eqs. (5) and (6) (see text) to the experimental data for $T > 100$ K.

The results displayed in Fig. 11 clearly show that for $Eu_{1-x}Y_xMnO_3$, with $x=0$, 0.3, and 0.4, there is only a faint frequency shift at T_N in the temperature dependence of the phonon frequency from the normal anharmonic behavior. In contrast to this, a significant negative frequency shift is found for $x=0.2$ and an observable negative and positive shifts are observed for $x=0.1$ and $x=0.5$, respectively.

For all these compounds the shifts appear well above the onset of the magnetic order and consequently it is very unlikely that these effects are driven by any kind of long-range spin ordering. It may be that the shifts occur when the temperature allows some kind of local order concerning the spins which can be probed by Raman scattering, as it will be discussed at the end of this work.

The frequency shift of a given phonon as a function of temperature, due to the spin-phonon coupling, is determined by the spin-spin correlation function,[34,35]

$$\omega = \omega_o + \gamma\langle\vec{S}_i \cdot \vec{S}_j\rangle, \tag{7}$$

where ω is the renormalized phonon frequency at a fixed temperature, ω_o denotes the frequency in the absence of spin-phonon coupling, and γ is the spin-phonon coupling constant.

When there are ferromagnetic and antiferromagnetic competitive interactions, it was proposed for the frequency shift,[35,36]

$$\omega - \omega_o \propto -R_1\langle\vec{S}_i|\vec{S}_j\rangle + R_2\langle\vec{S}_i|\vec{S}_k\rangle, \tag{8}$$

where R_1 and R_2 are spin-dependent force constants of the lattice vibrations deduced as the squared derivatives of the

exchange integrals with the respect to the phonon displacement. R_1 is associated with the ferromagnetic nearest neighbor and R_2 is associated with the antiferromagnetic next-nearest neighbor exchange.[35] The magnetic properties are determined dominantly by the exchange integrals, which depend on the number of ferromagnetic and antiferromagnetic interactions in the system. This model predicts negative or positive frequency shifts depending on the relative strength between the ferromagnetic and antiferromagnetic exchange interactions, associated with the eigenmode being considered. In the grounds of the model presented to above, the Raman frequency shifts displayed in Fig. 11 will be interpreted by assuming the coexistence of ferromagnetic and antiferromagnetic competitive exchange interactions, and spin-phonon coupling in the $Eu_{1-x}Y_xMnO_3$ system. As it has been assumed in current literature, we consider that the spin correlation functions of the nearest neighbors and the next-nearest neighbors have almost the same temperature dependence,[37] and thus, we take the same correlation functions for $\langle \vec{S}_i | \vec{S}_j \rangle$ and $\langle \vec{S}_i | \vec{S}_k \rangle$. Moreover, as we are dealing with the same eigenmode, we also assume constant values for R_1 and R_2. So, Eq. (8) can be written as follows:

$$\omega - \omega_o \propto (R_2 - R_1)\langle \vec{S}_i | \vec{S}_j \rangle. \tag{9}$$

For $x=0$, 0.1, and 0.2, the Raman shift is negative, increasing as the x value increases up to 0.2, where it takes its maximum value. This means that the difference R_2-R_1 becomes more negative with x up to 0.2. For $x=0.3$, the Raman frequency shift is also negative, but with a small value. On the other hand, for $x=0.4$ and 0.5 a clear positive Raman shift is observed. It worth to stress that the weak ferromagnetic character of the compounds with x between 0 and 0.2 cannot be explain by this model, as it is associated with the number of the exchange integrals and not with the second derivatives to the phonon displacements, represented by the R_1 and R_2 coefficients. This in good agreement with fact that the ferromagnetic features in these compounds arise below 45–28 K, depending on x (see phase diagram in Fig. 1), which is far below 100 K where the spin-phonon coupling mechanism emerges.

Except for $EuMnO_3$, the linewidth deviates, around 100 K, from the purely anharmonic temperature dependence behavior. For $x=0.20$, the linewidth presents a further anomaly at $T_N \approx 50$ K where the temperature derivative of the wave number is maximum. A similar analysis of the other Raman bands was performed and the results show that the shifts are less pronounced for these modes than for the symmetric one.

Through out of the scope of this work, it is worth to note the kink at ~250 K in the temperature behavior of the SS mode frequency for $x=0.4$ [see Fig. 11(e)]. However, a detailed analysis of this issue will be presented in a forthcoming work.

C. Spin-phonon coupling toward polar and magnetoelectric properties of $Eu_{0.8}Y_{0.2}MnO_3$

$Eu_{0.8}Y_{0.2}MnO_3$ is one member of the $Eu_{1-x}Y_xMnO_3$ system, which has been reported by Hemberger *et al.*[13] as one of the rather rare multiferroic materials, wherein ferroelectricity and ferromagnetism coexist below $T_{AFM\text{-}3}=22$ K. Moreover, the temperature dependence of the octahedral symmetric stretching mode, referred to above, revealed an impressive downward shift below to ~100 K relatively to the expected temperature behavior associated to nonlinear thermal processes. In order to figure out the mechanisms which yield the observed behavior of $Eu_{0.8}Y_{0.2}MnO_3$, we carried out measurements of its polar and magnetoelectric properties. Figure 12 shows the hysteresis loops obtained at several selected temperatures. Between 40 and 28 K, a linear $P(E)$ dependence is observed. As the temperature decreases from 27 K toward 23 K, hysteresis loops can be detected, with an elongated shape. A saturation value of the electric polarization could not be achieved, even for electric fields of up to 15 kV/cm, which shows how easily this material can be polarized.[21] The most remarkable result is the retrieval of the linear $P(E)$ relationship below $T_{AFM\text{-}3}$, which clearly reveals that ferroelectricity is intrinsic in the AFM-2 magnetic phase, and not in the AFM-3 phase, as previously suggested by Hemberger *et al.*[13]

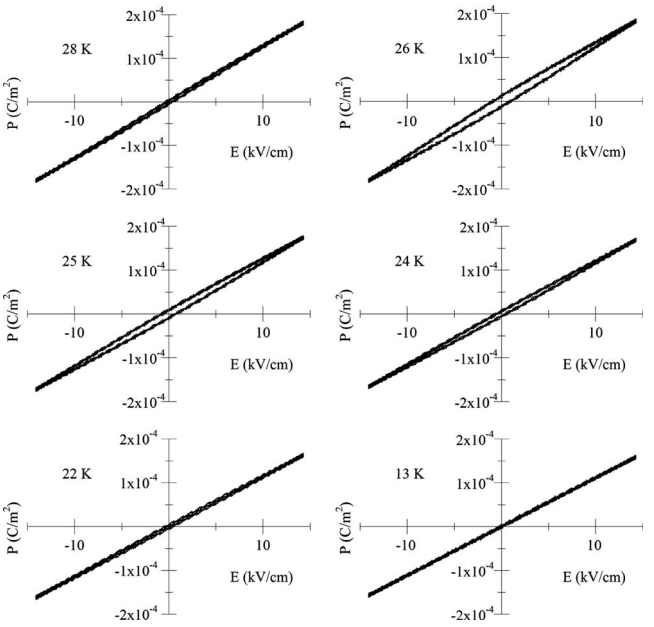

FIG. 12. $P(E)$ recorded at 330 mHz, for fixed different temperatures.

The measurement of pyroelectric current was carried out as follows: a low-poling electric field ($E_p \approx 0.001$ kV/cm) was applied inside the ferroelectric phase ($T=25$ K).

It is convenient to stress that we have used an enough lower dc electric field intensity, which allows both enhancing the alignment of the spontaneous ferroelectric dipoles, and minimizing the induced electric polarization arising from other potential dipolar systems, which may be already present in the material. After poling, the electric field was removed, and the sample cooled down to 10 K. A short circuit was then carried out for ~30 min. Measurements of the electric current were performed in a heating run without applied electric field. Figure 13(a) shows the pyroelectric current density (J_p) as a function of the temperature. Anomalies are detected at both $T_{AFM\text{-}2}=30$ K and at $T_{AFM\text{-}3}=22$ K,

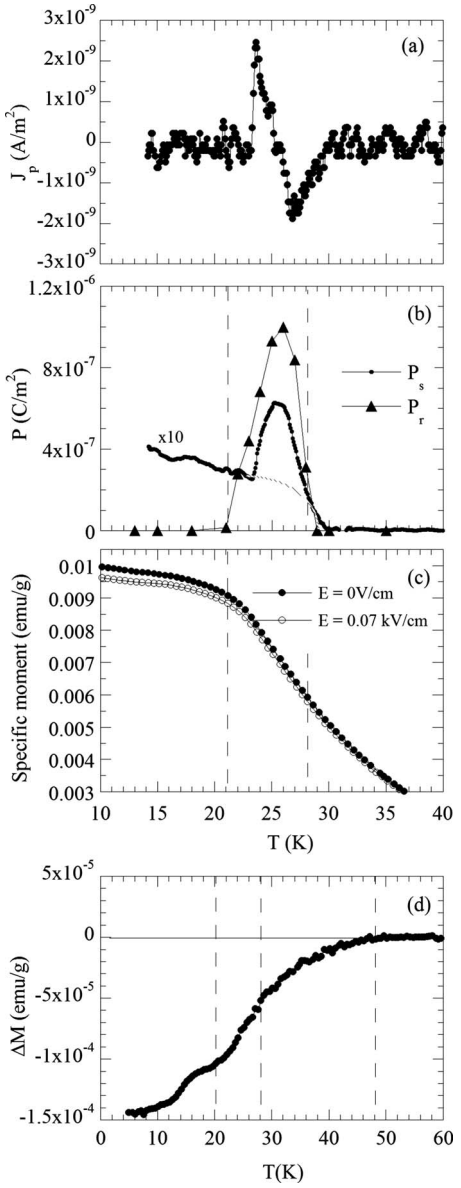

FIG. 13. (a) Temperature dependence of the pyroelectric current density, measured in a heating run, after cooling the sample with an applied electric field 1 V/cm. (b) Temperature dependence of the electric polarization (P) obtained from the time integration of the pyroelectric current, and of the remanent polarization (P_r), obtained from the $P(E)$. (c) Temperature dependence of the specific magnetization measured in heating run after cooling the sample under an electric field of 0 V/cm and 0.07 kV/cm. (d) Temperature dependence of the difference of the magnetization, measured under electric field and zero electric field cooling conditions.

with opposite signs, yielding a spontaneous component for the electric polarization (P_s) between T_{AFM-3} and T_{AFM-2}. We calculated the electric polarization (P) by time integrating the pyroelectric current density, which is presented in Fig. 13(b). The analysis of the data displayed in Fig. 12, yields the temperature dependence of the remanent polarization (P_r), shown in Fig. 13(b) along with $P_s(T)$. As it is general the case, the amplitude of the P_r obtained from hysteresis loops is larger than that obtained from the analysis of the

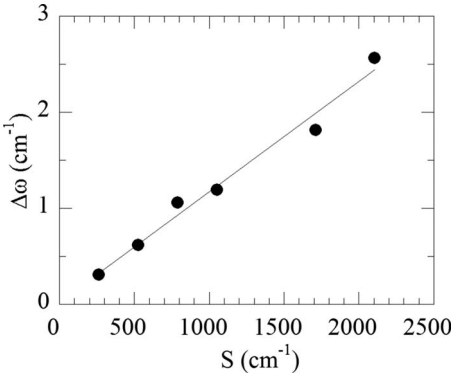

FIG. 14. Frequency deviation from the extrapolated temperature behavior for $T>100$ K, of the symmetric stretching mode of $Eu_{0.8}Y_{0.2}MnO_3$, versus the spectral weight calculated from the terahertz data, below 140 cm^{-1}, for the sample $Eu_{0.75}Y_{0.25}MnO_3$ (Ref. 17). The straight line is a guide for the eyes.

pyroelectric current. Leaving out the tail of $P_s(T)$ observed below T_{AFM-3}, which is apparently associated with the induced polarization component already observed just below $T_{AFM2}=30$ K, the occurrence of both P_s and P_r between T_{AFM-2} and T_{AFM-3}, provides clear evidence for the ferroelectric character of the AFM-2 phase. Actually, to classify a phase as a ferroelectric one, observing just one of the two aforementioned quantities is not enough. Contrarily, both of them have to occur in the same phase.

Figure 13(c) shows the temperature dependence of the induced magnetization measured under both zero and nonzero polarizing electric field cooling conditions. In order to gain a deeper knowledge of the effect of the electric field on the magnetic system, we have determined the temperature dependence of the difference of the magnetization (ΔM), measured under electric field and zero electric field cooling conditions, which is displayed in Fig. 13(d). The effect of the polarizing electric field in the magnetization starts to be visible only in the ordered magnetic phases. It increases as the temperature decreases, sensing the phase transitions both at T_{AFM-2} and T_{AFM-3}, by either small steps or changes in the curvature. As can be seen, an electric field as low as 0.07 kV/cm yields a significant decrease in the induced magnetization magnitude below T_{AFM-2}, reaching a 5% reduction at the lowest temperature. The temperature dependence of ΔM can be well understood from the ordering of the magnetic structure occurring below T_N, along with the spin-lattice coupling mechanism already present below 100 K.

V. DISCUSSION AND CONCLUDING REMARKS

In this work we have presented a systematic study concerning the structure at room temperature and the phonon behavior at low temperatures in orthorhombic $Eu_{1-x}Y_xMnO_3$ manganites.

The structural data obtained from both x-ray diffraction and Raman-scattering experiments reveal orthorhombic deformations due to a strong cooperative Jahn-Teller distortion, which increases with increasing Y^{3+} substitution rate. In the Raman-scattering data, the lattice distortions manifest them-

selves by frequency shifts of both the tilt and the bending modes of the MnO_6 units, modifications of the mode coupling, enhancement of the energy-transfer mechanisms between modes, and increase in the Raman band linewidths. The data analysis points at a correlation between the x dependence of the more intense Raman bands with the Mn-O bond lengths, and the Mn-O(I)-Mn bond angle; i.e., the stretching modes (symmetric and antisymmetric) correlate to Mn-O bonds, while bending and tilt mode are associated with the Mn-O(I)-Mn angle. The study of Raman spectra as a function of the temperature, in the mixed polycrystalline $Eu_{1-x}Y_xMnO_3$ ($0 \leq x \leq 0.50$) reveals a shift in the temperature dependence of the phonon frequency away from the normal anharmonic behavior, particularly significant for $x=0.20$. The frequency shift, due to the spin-phonon coupling interaction, regarding to the pure anharmonic temperature dependence of the phonon frequency, is positive or negative depending on the x values. This behavior can be understood in terms of a competition between ferromagnetic and antiferromagnetic interactions, revealed through the existence of modulated structures in the low-temperature phases of these materials.

As we will see in the following, our Raman results correlate very well with experiments of the terahertz transmittance on $Eu_{1-x}Y_xMnO_3$.[17,18] The analysis obtained from these experiments revealed the existence of electromagnons in samples with $x=0.20$, 0.30, and 0.50, providing information about the static dielectric constant below T_1, and also providing evidenced for a broad background absorption observed up to T_N+50 K. In our Raman work, we have observed a deviation of the frequency from the anharmonic behavior, well above the magnetic phase transition, associated with the spin-phonon coupling mechanism referred to above. Laverdière *et al.*[10] also have observed a softening for A_g and B_{2g} stretching modes in, e.g., $NdMnO_3$ and $DyMnO_3$, starting well above T_N, which they relate to a small expansion in the Mn-O distance rather than to a spin-phonon coupling. However, if we consider that manganites are well known for their often peculiar local structure in terms of electronic and magnetic properties, it is also plausible to associate this type of behavior with local magnetic fluctuations, similarly to that was proposed in rare-earth nickelates.[38–40] Aguilar *et al.*[17] have associated the existence of the background absorption in the terahertz region of the paramagnetic phase with the coupling between phonons and electromagnons. We have reconsidered the correlation between the total spectral weight below 140 cm^{-1}, depicted in Fig. 2 of Ref. 17, and the frequency shift calculated from our results for $x=0.20$. The results are displayed in Fig. 14. They provide support for a mechanism that involves spin-spin coupling, since the shift of the measured frequency (proportional to $\vec{S}_i \cdot \vec{S}_j$) for $x=0.20$ scales rather well with the spectral weight displayed in Fig. 2 of Ref. 17, in the temperature range 50–100 K. This spectral weight, calculated from the sample with $x=0.25$, is reported to be proportional to the coupling of phonons to the electromagnon of the magnetic system, in the paramagnetic phase, i.e., also proportional *to* $\vec{S}_i \cdot \vec{S}_j$. As expected, the scaling found is independent of yttrium content but the factor of proportionality between the shift of frequency and the spectral weight is actually not. In a recent paper, Issing *et al.*[41] discussed spin-phonon coupling in the same system, referring to contradicting results regarding the way softening of internal modes of MnO_6 units depends on yttrium content for both single crystals and granular samples. The excellent correlation presented in Fig. 14 between phonon softening and electromagnon yields in fact a distinctly dependence on yttrium content as opposed to that is referred to in Ref. 41. Furthermore, our results are still in very good agreement with lattice studies carried out in single crystals of other similar materials.[10] Thus, the results presented in this work are not strictly affected by the granular nature of our samples.

We have also investigated the polar and magnetoelectric character of the singular case of the $Eu_{0.8}Y_{0.2}MnO_3$ composition. Our results clearly show that the AFM-2 phase is definitely ferroelectric, though with very small values of the spontaneous polarization, likely stemming from lattice deformations resulting from the mechanisms associated with the phase transition at $T_{AFM\text{-}2}$. A significant electric field induced magnetization change $\Delta M(T)$ was put in evidence just below T_N, as a consequence of both the spin-lattice coupling mechanism existing already below ~100 K, and the emerging order of the magnetic structure below to the Néel temperature.

ACKNOWLEDGMENTS

This work was supported by Fundação para a Ciência e Tecnologia, through the Project No. PTDC/CTM/67575/2006 and by Program Alßan, the European Union Program of High Level Scholarships for Latin America (Scholarship No. E06D100894BR). J. Kreisel thanks the European STREP MaCoMuFi for financial support.

*jamoreir@fc.up.pt

[1] N. A. Hill, J. Phys. Chem. B **104**, 6694 (2000).
[2] W. Eerenstein, N. D. Mathur, and J. F. Scott, Nature (London) **442**, 759 (2006).
[3] R. E. Cohen, Nature (London) **358**, 136 (1992).
[4] T. Kimura and Y. Tokura, J. Phys.: Condens. Matter **20**, 434204 (2008).
[5] J. L. Ribeiro, Phys. Rev. B **76**, 144417 (2007).
[6] M. Kenzelmann, A. B. Haris, S. Jonas, C. Broholm, J. Schefer, S. B. Kim, C. L. Zhang, S. W. Cheong, O. P. Vajk, and J. W. Lynn, Phys. Rev. Lett. **95**, 087206 (2005).
[7] T. Kimura, G. Lawes, T. Goto, Y. Tokura, and A. P. Ramirez, Phys. Rev. B **71**, 224425 (2005).
[8] I. A. Sergienko and E. Dagotto, Phys. Rev. B **73**, 094434 (2006).
[9] M. Mostovoy, Phys. Rev. Lett. **96**, 067601 (2006).
[10] J. Laverdière, S. Jandl, A. A. Mukhin, V. Yu. Ivanov, V. G.

Ivanoc, and M. N. Iliev, Phys. Rev. B **73**, 214301 (2006).
[11] J. Hemberger, A. Krimmel, T. Kurz, H.-A. Krung von Nidda, V. Y. Ivanov, A. A. Mukhin, A. M. Balbashov, and A. Loidl, Phys. Rev. B **66**, 094410 (2002).
[12] V. Yu. Ivanov, A. A. Mukhin, V. D. Travkin, A. S. Prokhorov, A. M. Kadomtseva, Y. F. Popov, G. P. Vorob'ev, K. I. Kamilov, and A. M. Balbashov, Phys. Status Solidi B **243**, 107 (2006).
[13] J. Hemberger, F. Schrettle, A. Pimenov, P. Lunkenheimer, V. Yu. Ivanov, A. A. Mukhin, A. M. Balbashov, and A. Loidl, Phys. Rev. B **75**, 035118 (2007).
[14] J. A. Alonso, M. J. Martínez-Lope, M. T. Casais, and M. T. Fernández-Díaz, Inorg. Chem. **39**, 917 (2000).
[15] T. Goto, T. Kumira, G. Lawes, A. P. Ramirez, and Y. Tokura, Phys. Rev. Lett. **92**, 257201 (2004).
[16] Y. Yamasaki, S. Miyasaka, T. Goto, H. Sagayama, T. Arima, and Y. Tokura, Phys. Rev. B **76**, 184418 (2007).
[17] R. Valdés Aguilar, A. B. Sushkov, C. L. Zhang, Y. J. Choi, S.–W. Cheong, and D. Drew, Phys. Rev. B **76**, 060404(R) (2007).
[18] A. Pimenov, A. Loidl, A. A. Mukhin, V. D. Travkin, V. Yu. Ivanov, and A. M. Balbashov, Phys. Rev. B **77**, 014438 (2008).
[19] T. Mori, N. Kamegashira, K. Aoki, T. Shishido, and T. Fukuda, Mater. Lett. **54**, 238 (2002).
[20] J. Agostinho Moreira, A. Almeida, M. R. Chaves, M. L. Santos, P. P. Alferes, and I. Gregora, Phys. Rev. B **76**, 174102 (2007).
[21] J. Agostinho Moreira, A. Almeida, W. S. Ferreira, M. R. Chaves, S. M. F. Vilela, P. B. Tavares, B. Kundys, R. Ranjith, and W. Prellier, J. Appl. Phys. **107**, 024108 (2010).
[22] J. Agostinho Moreira, A. Almeida, W. S. Ferreira, M. R. Chaves, B. Kundys, R. Ranjith, W. Prellier, S. M. F. Vilela, and P. B. Tavares, J. Phys.: Condens. Matter **21**, 446002 (2009).
[23] M. N. Iliev and M. V. Abrashev, J. Raman Spectrosc. **32**, 805 (2001).
[24] A. M. Glazer, Acta Crystallogr., Sect. B: Struct. Crystallogr. Cryst. Chem. **28**, 3384 (1972).
[25] P. M. Woodward, T. Vogt, D. E. Cox, A. Arulraj, C. N. R. Rao, P. Karen, and A. S. K. Cheetham, Chem. Mater. **10**, 3652 (1998).
[26] J. Rodriguez-Carvajal, M. Hennion, F. Mausa, A. H. Mondden, L. Pinsard, and A. Revcolevschi, Phys. Rev. B **57**, R3189 (1998).
[27] J. Petzelt, T. Ostapchuk, I. Gregora, I. Rychetský, S. Hoffmann-Eifert, A. V. Pronin, Y. Yuzyuk, B. P. Gorshunov, S. Kamba, V. Bovtun, J. Pokorný, M. Savinov, V. Porokhonskyy, D. Rafaja, P. Vaněk, A. Almeida, M. R. Chaves, A. A. Volkov, M. Dressel, and R. Waser, Phys. Rev. B **64**, 184111 (2001).
[28] L. Martín-Carrón, A. de Andrés, M. J. Martínez-Lope, M. T. Casais, and J. A. Alonso, Phys. Rev. B **66**, 174303 (2002).
[29] M. N. Iliev, M. V. Abrashev, J. Laverdière, S. Jandl, M. M. Gospodinov, Y.-Q. Wang, and Y.-Y. Sun, Phys. Rev. B **73**, 064302 (2006).
[30] M. N. Iliev, M. V. Abrashev, H. G. Lee, V. N. Popov, Y. Y. Sun, C. Thomsen, R. L. Meng, and C. W. Chu, Phys. Rev. B **57**, 2872 (1998).
[31] V. A. Amelitchev, B. Güttler, O. Yu. Gorbenko, A. R. Kaul, A. A. Bosak, and A. Yu. Ganin, Phys. Rev. B **63**, 104430 (2001).
[32] M. Rini, R. Tobey, N. Dean, J. Itatani, Y. Tomioka, Y. Tokura, R. W. Schoenlein, and A. Cavalleri, Nature (London) **449**, 72 (2007).
[33] M. Balkanski, R. F. Wallis, and E. Haro, Phys. Rev. B **28**, 1928 (1983).
[34] D. J. Lockwood and M. G. Cottam, J. Appl. Phys. **64**, 5876 (1988).
[35] W. Baltensperger and J. S. Helman, Helv. Phys. Acta **41**, 668 (1968).
[36] K. Wakamura and T. Arai, J. Appl. Phys. **63**, 5824 (1988).
[37] H. B. Callen and E. Callen, Phys. Rev. **136**, A1675 (1964).
[38] J. M. Wesselinowa and A. T. Apostolov, J. Phys.: Condens. Matter **8**, 473 (1996).
[39] C. Girardot, J. Kreisel, S. Pignard, N. Caillault, and F. Weiss, Phys. Rev. B **78**, 104101 (2008).
[40] G. Catalan, Phase Transitions **81**, 729 (2008).
[41] S. Issing, A. Pimenov, V. Yu. Ivanov, A. A. Mukhin, and J. Geurts, Phys. Rev. B **81**, 024304 (2010).